Title

Real-time interface investigation on degradation mechanism of organic light-emitting diode by in-operando X-ray spectroscopies

Authors

Nie, Kaiqi
Zhang, Hui
McLeod, John A
et al.

Publication Date

2020-12-01

DOI

10.1016/j.orgel.2020.105901

Peer reviewed

Real-time Interface Investigation on Degradation Mechanism of Organic Light-emitting Diode by In-operando X-ray Spectroscopies

Kaiqi Nie,[†,#,‡] Hui Zhang,[†,#,§,‡] John A. McLeod,[†,‡] Duo Zhang,[†] Dongying Zhou,[†,‖] Yujian Xia,[†] Jun Zhong,[†] Liangsheng Liao,[†] Jinghua Guo,[, #,⊥] and Xuhui Sun[*,†]*

[†] Institute of Functional Nano & Soft Materials (FUNSOM), Jiangsu Key Laboratory for Carbon-Based Functional Materials & Devices, Joint International Research Laboratory of Carbon-Based Functional Materials and Devices, Soochow University, Suzhou 215123, P. R. China.

Advanced Light Source, Lawrence Berkeley National Laboratory, Berkeley, CA 94720, USA

[§] State Key Laboratory of Functional Materials for Informatics, Shanghai Institute of Microsystem and Information Technology, Chinese Academy of Sciences, Shanghai 200050, P. R. China.

[‖] Soochow Institute for Energy and Materials InnovationS (SIEMIS), College of Physics, Optoelectronics and Energy, Soochow University, Suzhou 215006, P. R. China.

[⊥] Department of Chemistry and Biochemistry, University of California, Santa Cruz, CA 95064, USA.

*Corresponding Author E-mail address: xhsun@suda.edu.cn, jguo@lbl.gov.

Abstract: Understanding the chemical evolution at the interface of organic light-emitting diodes (OLEDs) under working conditions is critical for addressing device failure and further improving performance. In this work, an in-operando approach was developed employing synchrotron-based X-ray absorption spectroscopy (XAS) to investigate the electronic structures and chemical degradation mechanisms of a model tris(8-hydroxyquinoline) aluminum (Alq_3)-based OLED device under working condition. The results identify that Mg

atoms from the electrode migrate into the Alq_3 organic layer under a potential bias and replace Al atom sites, forming the unstable Mgq_3 species which lead to device degradation. The findings from the classic and simple model device elucidate the degradation mechanisms occurred at the interface of OLED devices, which may facilitate the development of more efficient and stable OLED devices with complex structures.

Keywords: organic light-emitting diode, in-operando, X-ray absorption spectroscopy, interface interaction, degradation mechanism

1. Introduction

Organic light-emitting diodes (OLEDs) have stridden forward to the commercialization in various applications, such as flat panel displays and solid-state lighting, due to their unique features including high brightness, large viewing angle, simple manufacturing process, and excellent flexibility,[1] etc. However, optimizing performance and improving the long-term operational stability of OLEDs is still an area of active research. Although there have been tremendous developments in OLED research, electronic structure evolution at the interface and chemical degradation in OLEDs are still major unsolved problems. Intrinsic degradation is characterized by the decrease of overall luminance over time during continuous operation, and can be recognized by analysis of the noise fluctuations when the OLED is operated.[2] This type of degradation is attributed mainly to the deterioration of organic or metal-organic molecules in the device.[3] The location and nature of this chemical degradation are highly dependent on the employed materials as well as the device configuration. However, the complexity of chemical bond dissociation makes the degradation process, to a large extent, still a “black box”. Insight into this challenging problem requires a fundamental understanding of the electronic structure evolution of the organic layers during degradation. Most extant degradation mechanism studies have been performed by disassembling the

devices, dissolving the organic materials, and subsequently analyzing the solutions by different techniques such as nuclear magnetic resonance (NMR)[4, 5] and time-of-flight mass spectrometry (TOF-MS).[6] In addition, of those studies regarding OLED degradation available in the literatures, most are based on the component materials considered in isolation, and not on the device architecture.[7] Consequently, whether the material studied ex-situ is still in the same state as when it was functioning in the device is an open question. On the other hand, for studies of actual devices, the typical in-operando characterization methods such as photoluminescence (PL) and electroluminescence (EL) spectroscopy[8, 9] cannot provide direct evidence of chemical degradation, but only qualitative comparisons can be obtained. To enable the development of novel materials with better performance and stability, it is crucial to learn the chemical nature of defects in the organic layers of OLED device and the possible chemical reactions under the working conditions that lead to the degradation.

To clearly understand the chemical degradation mechanisms in OLEDs, an in-operando technique is necessary to detect the interface reactions during operation. However, laboratory-based XPS or ultraviolet photoelectron spectroscopy (UPS) cannot be applied to characterize the degradation mechanism of OLEDs under working conditions, not only due to the short photoelectron penetration depth but also because surface charging effects during operation leads to unknown photoelectron energy shifts. Synchrotron-based soft X-ray absorption spectroscopy (XAS) and X-ray emission spectroscopy (XES) have the capability to probe the unoccupied and occupied electronic structure of materials with elemental selectivity,[10] for example, Kim et al.[11] investigated the highest occupied molecular orbital (HOMO) and lowest unoccupied molecular orbital (LUMO) of tris(8-hydroxyquinoline) aluminum (Alq_3) film on a Si wafer substrate by measuring C K-edge X-ray spectroscopy. Curioni et al.[12] used the density functional theory (DFT) to calculate the XAS and X-ray photoelectron spectroscopy (XPS) spectra of Alq_3, which divulge information on the density of states

(DOS). Owing to the unique properties of photon-in/photon-out spectroscopy, XAS based on total fluorescence yields (TFY) mode and XES are promising in-operando tools to detect the electronic structure evolution of an OLED device by the fluorescence emitted photons which could probe the interface through the topmost metal electrode. To-date, these techniques are under-utilized by the OLED community, probably due to the complexities of arranging an in-operando synchrotron experiment and concern of sample damage exposing to high photon flux, which could be mitigated as discussed in the later section.

In the present work, in order to understand the interfacial phenomena occurring in complex OLED structures and the chemical degradation mechanisms therein, we performed a systematic investigation of the electronic structure of Alq_3 (representative of a typical active organic material) in an OLED device as a model system by in-operando soft X-ray spectroscopies. The interface interactions between Alq_3 and metal atoms from the cathode were also examined. Our approach represents a flexible method for investigating electronic structure variations in OLED active layers in-operando. Interface reaction is a crucial issue to all kinds of organic optoelectronic devices; thus, we selected the classic and simple model of Alq_3 to illustrate the common metal/organic interfaces in the device. The result provides insight on strategies to improve the stability and performance of OLEDs with complex structures in general.

2. Results and Discussion

2.1. In-operando XAS measurement of OLED device

A typical two-layered OLED device for in operando XAS study was shown in **Figure 1**. The device was fabricated on commercial indium tin oxide (ITO) coated glass as the anode electrode. A 45 nm N,N'-bis(1-naphthalenyl)-N,N'-bisphenyl-(1,1'-biphenyl)-4,4'-diamine (NPB) film was thermally evaporated on the top of the ITO surface to obtain a hole injection

and transport layer. Subsequently, 55 nm Alq_3 was deposited as both the emitting and electron transport layer. In the final step, Al or MgAg (10:1, wt%) metal was evaporated on the top layer as a cathode electrode. The thickness of each layer in the device was monitored by an in-situ quartz crystal monitor (QCM) and all thickness of the layers was optimized by considering both the X-ray penetration length and the device performance. The 50 nm thick metal electrode is sufficient to be a uniform cathode layer while also allowing for X-ray penetration in our photon-in, photon-out measurements to observe the X-ray signal from the underlying Alq_3 layer. The device of in-operando XAS study was encapsulated into glass vessel for shipment to the synchrotron beamline station and then assembled onto a unique in-operando holder as shown in Figure S1 (Supporting Information) in an Ar glove box.

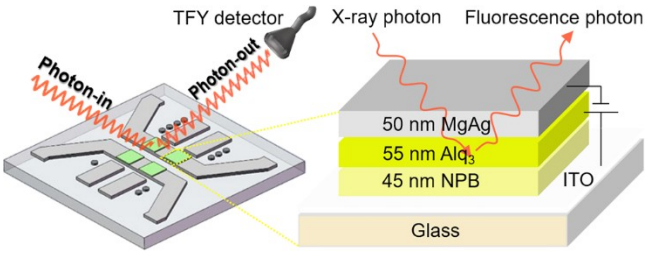

Figure 1. Schematic diagram of the in-operando XAS experimental setup and the cross-sectional scheme of the ITO/NPB/Alq_3/MgAg device.

As there are nine different carbon sites in an Alq_3 molecule as shown in Figure S2 (Supporting Information) and oxygen is unfortunately an ever-present contamination, nitrogen is the most appropriate element to monitor the chemical changes of Alq_3 during the device operation. Therefore, N in Alq_3 is expected to be more sensitive with the chemical response for the in-operando measurement. As displayed in Figure S3 (Supporting Information), the N K-edge XAS spectral profiles of Alq_3 are in good agreement with previous studies.[11, 12] The intense peak at 399 eV originates from the π* resonance feature of N atom in π ring. Since there is no N atom in the π ring of NPB molecule as shown in Figure S2a (Supporting Information), this π* resonance feature is very weak in the N K-edge XAS spectra of NPB.

Therefore, the N signal from the underlying NPB layer could be easily attenuated and excluded from the measurement of the entire OLED device. Essentially, all of the π* feature can be attributed to the Alq_3; and consequently, the changes in this feature during device operation reflect the chemical evolution in the partial DOS (pDOS) of Alq_3.

As shown in **Figure 2**a, the in-operando N K-edge XAS of the OLED device with a MgAg cathode show up an obvious change in π* feature under working conditions: a new shoulder feature arises near 400 eV which is not present in the as-synthesized device, indicating the different chemical environment. The N K-edge XAS spectra acquired under working conditions can be deconvoluted into three components: the violet curve at 399 eV in Figure 2a corresponding to the well-known main π* resonance feature present in all Alq_3 spectra. The pre-edge feature deconvoluted as yellow curve around 398.5 eV will be discussed in the later section. The green curve at 400 eV in Figure 2a corresponding to a new state resulting from the chemical environment changes under working conditions. We trace the origin of this new state as follows. The shoulder species around 400 eV manifests under working conditions (labeled "Working (on)") and persists even without bias (labeled "Working (off)") although decrease in intensity, and becomes more intense until the device failure (labeled "Broken"). These spectral changes are the significant fingerprint of the degradation mechanism for Alq_3-based OLED devices. This evolution in the N K-edge XAS spectra indicates an interface reaction involving the nitrogen functional group during operation.

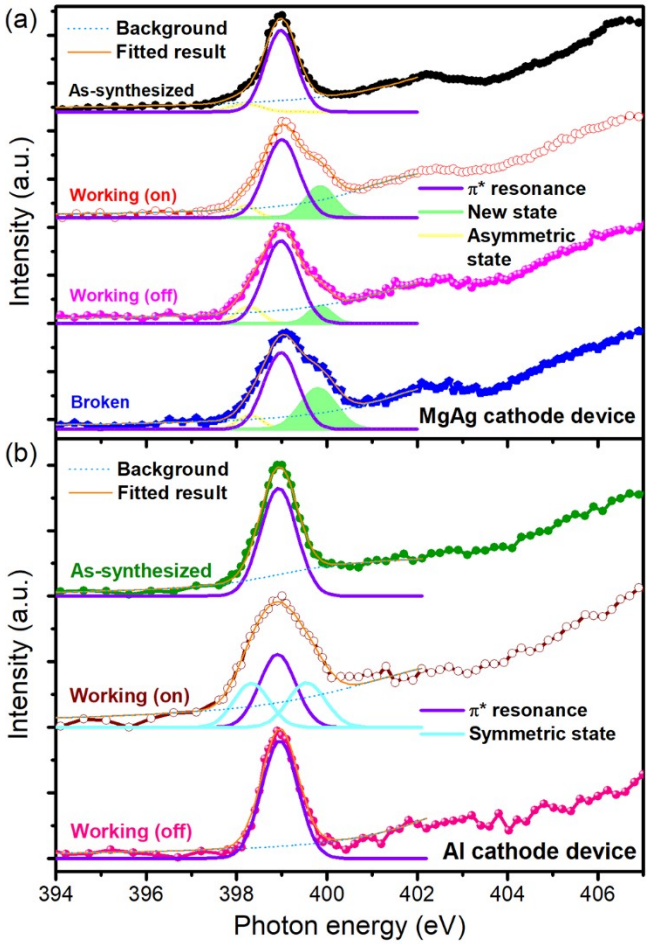

Figure 2. a) N K-edge XAS of an ITO/NPB/Alq_3/MgAg OLED device as-synthesized, under bias ("Working (on)"), after bias is removed ("Working (off)"), and after device failure ("Broken"). The curve in violet indicates the nitrogen in π ring, while the curve in green corresponds to the new state appeared upon device operation, together with a pre-edge component in yellow curve. b) N K-edge XAS of an ITO/NPB/Alq_3/Al OLED device as-synthesized, under bias ("Working (on)") and after bias is removed ("Working (off)"). Two symmetric component in light blue curve can be found in working on device with Al electrode.

We then confirmed this proposed mechanism by performing a control experiment in which the MgAg electrode was replaced with a pure Al electrode. Based on previous molecular dynamics simulations,[13] Alq_3 molecules should not be decomposed during Al deposition, and only weak bonding occurs between the deposited Al electrode and the N, O atoms in Alq_3 and their molecular structures remain essentially intact with weak Al-N and Al-O bonds. Therefore, pure Al metal is a favorable cathode to confirm our proposed cathode-side interface (MgAg/Alq_3 interface) reaction. To maintain a driving current at 5 mA (consist

with MgAg cathode device operation), a higher bias was needed to drive the Al cathode device (as shown in Figure S4, Supporting Information) due to the higher work function of Al cathode than MgAg (10:1) cathode.[14] This higher bias leads to more electrons accumulating at the Alq_3/Al interface[15] than Alq_3/MgAg interface with lower bias. When the current passed through the device, Alq_3 was excited and the exciton pairs were formed, either in singlet or triplet. Consequently, the exciton recombination took place within the ligand with light emitting. The comparatively inefficient injection of electrons into Alq_3 from the Al interface of high work function leads to a higher density of unstable species in charge state adjacent to the Alq_3/Al interface compared to the Alq_3/MgAg interface. As shown in Figure 2b, the N K-edge XAS spectrum of the Al cathode device suffers from the greater symmetric peak broadening during in-operando measurement than that of the as-synthesized Al cathode device. As the Alq_3 molecules become distorted under operation with external bias,[16] the symmetric state around the π^* resonance might be due to the interference of electron accumulation at the Alq_3/Al cathode interface with the high work function,[17] these accumulated electrons may enter carrier-trapping gap states or undergo exciton quenching at the Alq_3/Al cathode interface,[18] which will be discussed more in the later section. As expected, this peak broadening is completely reversible after the bias is removed, as shown in the spectrum from the Al cathode device after operation (labeled “Working (off)”). There is not the asymmetric shoulder species at 400 eV observed in all the spectra of Alq_3/Al electrode interface, indicating that the shoulder species can be related to an interface reaction between MgAg electrode and Alq_3 during operation.

Al K-edge XAS measurements were also performed for MgAg cathode devices to confirm our proposed mechanism from another point of view at the Al site. As shown in Figure S5, Supporting Information, the Al K-edge XAS spectra from both a pristine Alq_3 thin film on ITO and an as-synthesized ITO/NPB/Alq_3/MgAg OLED device exhibit a flat pre-edge

region. A pre-edge feature around 1555 eV manifests in the spectrum of the OLED under working conditions (labeled "Working") which can be assigned to a defect state. This pre-edge feature becomes much more intense after device failure eventually (labeled "Broken"). Meanwhile, the Al K-edge spectra profile of the broken device looks similar to that of Al_2O_3, which indicate the degrading of Alq_3.[19]

2.2. Simulation results of Alq_3 OLED device

Based on our observation of the obvious new chemical state appearance only after the bias is applied to an Alq_3 OLED with MgAg cathode but not for Al cathode device, DFT simulations were performed to interpret the N K-edge XAS spectral variations. There are two stable isomers of Alq_3[20], i.e. meridional (mer) and facial (fac) as shown in Figure S2b of supplementary material. Both metastable adsorption structures of mer-/fac-Alq_3 were optimized and the electronic structures were calculated by using the SIESTA[21, 22] computer code, and more detailed parameter can be found in the supplementary material. As shown in Figure S6, Supporting Information, all the simulated X-ray absorption edges from Alq_3 are in good agreement with the experiment results.

The ITO/NPB/Alq_3/MgAg device exhibits an asymmetric trend to the low-energy direction in the N K-edge compared to ITO/Alq_3 as shown in Figure S3, Supporting Information, which influenced by the Mg atom diffusion during evaporation process.[23, 24] However, a new high-energy shoulder appears at 400 eV after the operation as stated above. X-ray beam-induced phenomenon is not responsible for these spectral changes, as the multiple successive spectra did not show obvious change of the π* resonance (as shown in Figure S7, Supporting Information). As illustrated in **Figure 3**a, when a Mg atom migrates near the Al-center, our calculations show that the LUMO shifts to lower energy (red shift) as shown in Figure 3b, consistent with previous simulations[25] and the observed experimental difference between the single Alq_3 film on ITO and an Alq_3 device. However, the observed

feature (400 eV) in the N K-edge XANES of the operating OLED device is shifted in the opposite direction. The interaction between the nitrogen lone pair electrons and the surrounding radicals in Alq_3 has been suggested as a source of material decomposition.[26] If the Al cation in Alq_3 is completely replaced by a Mg atom as demonstrated in Figure 3a which could take place under external bias, then the LUMO is shifted to the higher energy (blue shift) as shown in Figure 3b, in close agreement with the observed feature in the in-operando experimental spectra.

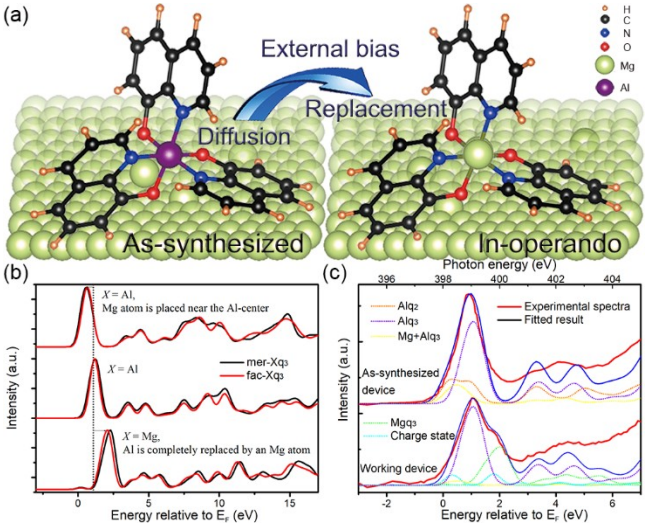

Figure 3. a) Schematic illustration of the Alq_3 molecular configuration at the MgAg cathode electrode interface. In the as-synthesized device, the Mg atom diffuses into the ligand of the Alq_3 molecule; then when under bias the Mg can completely replace the Al atom upon driven-bias under in-operando measurement. b) Theoretical N K-edge XAS simulation of an Alq_3 standard (middle); a Mg atom near the center of Alq_3 (top); and with Mg totally replacing the Al (bottom). All spectra are shifted vertically for clarity. c) N K-edge XAS of as-synthesized Alq_3 OLED device with MgAg electrode and under in-operando working condition together with the theoretical fitting result by the Alq_2, Alq_3, Alq_3 in charge state, Mgq_3 component and the situation that Alq_3 with an Mg atom near the Al center (denote as Mg+Alq_3).

To further clarify the reversibility phenomenon regarding the peak broadening of Al cathode device and the "new state" intensity decrease of MgAg cathode device in "working (off)" status, we also did investigation by simulating the Alq_3 charge state (denote positive/negative charge as $Alq_3^{+/-}$, respectively). As shown in Figure S8, Supporting Information, the N 2p pDOS of Alq_3^- shifts to the high-energy direction, while for Alq_3^+ it moves to the lower

position. The Alq_3 molecule adjacent to Al cathode can be interfered by the electrons accumulated at the interface due to the inefficient electron injection by the high work function cathode. Therefore, more Alq_3^- state in negative charge can be formed near the cathode interface, meanwhile Alq_3^+ charge state formed at the NPB/Alq_3 interface. The appearance as reversible π* resonance peak broadening after removal of the external bias, indicate the Alq_3 molecule revert back to its initial solid state without the charge injection and electric field. Besides, we should notice that Alq_3^- is formed at a relatively shallow depth, which is supposed to contribute more spectral weight.

Based on all the simulated DOS above, the N K-edge XAS spectra of MgAg device may be further qualitatively fitted by a superposition of pristine Alq_3, Mg+Alq_3 (Alq_3 with an Mg atom near the Al, the yellow curve in Figure 2a), "Mgq_3" (Alq_3 with the Al replaced with Mg), "Alq_2" (Alq_3 with one hydroxyquinoline group removed) which was calculated to be the more kinetically favorable species of "Alq_x" formed upon aging,[27] and "$Alq_3^{+/-}$" charge state as shown in Figure 3c. Moreover, intensity reversibility of the "new state" can be attributed to the partial overlapped Alq_3^- charge state with Mgq_3 species. Upon the removal of the external bias of the MgAg cathode device as shown in Figure 2a ("working (off)" status), the decrease of "new state" intensity can be attributed to the disappearance of overlapped Alq_3^- charge state and only Mgq_3 species state retain. On this basis of the spectra presented here, one can now characterize site-specific reactions or interactions that Alq_3 may undergo in a working device, and also identify the specific effects of chemical substitutions. Our work also presents a first-stage exploration which will offer the unique possibility to trace the charge interactions taking place in the working device, such as charge injection efficiency at the electrode/organic interface, which will ultimately help control and enhance the device performance.

3. Conclusion

In summary, a classic Alq_3-based OLED device was systematically studied by synchrotron-based X-ray spectroscopy and an in-operando approach to trace the real-time chemical evolution was developed. By measuring the N K-edge XAS spectra of OLED device under the working condition, the Mg atoms reacted with the Alq_3 evidently, instead of simply chemical absorbing onto the Alq_3 organic molecular layer like the as-synthesized device. Combined with the simulation and DFT calculation results, we find that at the interface, Mg migrates into the Alq_3 organic layer and even replaces the Al cation centers of the molecules when under external bias, forming the unstable Mgq_3 species. This Mgq_3 leads to the degradation of the entire OLED device. For this specific case, replacing Mg electrode with Al would mitigate degradation as the work function difference between metals affects the interface reaction. Moreover, an interlayer like LiF in between metal electrode and EML would generally help with improving the long term stability of OLED. Furthermore, XAS measures the unoccupied state which would give LUMO position. In the near feature, XAS would be applied to investigate the organic OLED material evaporation process layer by layer. Such result reveals the molecular orientation while thermal deposition, also affects band bending at the interface. A feasible energy alignment is crucial to improve the long term stability of an OLED. We believe that soft X-ray spectroscopy is a powerful tool for us to better understand the band structure of OLED. This first-stage in-operando soft X-ray investigation helps to understand the chemical degradation mechanisms of OLED devices and helps derive strategies for developing more effective and stable devices.

4. Experimental Section

Device fabrication: A schematic and a photograph of the sample holder for in-operando X-ray absorption measurement are shown in Figure S1, respectively. The sample holder was made of PEEK (polyetheretherketone) with two metal screw electrodes for bias control. After connecting the cathode and anode of the OLED to these screws by copper wire and applying

bias on the electrode, the OLED is powered through the connection to a potentiostat located outside the ultrahigh vacuum (UHV) chamber. In this study, the OLED was driven by a Keithley 2400-LV source-meter. By controlling the bias, we could tune the illumination intensity of the OLED. For comparison purposes, we fix the driving current to 5 mA for all in-operando measurements. The sample holder with device was transferred into the vacuum chamber at the beamline with a suitcase under the protection of Ar. A YAG (Yttrium aluminum garnet, $Y_3Al_5O_{12}$) crystal was placed for the X-ray alignment.

X-ray spectroscopy study: X-ray spectroscopy studies were performed at BL8.0.1.4 and BL6.3.1.2 of Advanced Light Source (Lawrence Berkeley National Laboratory). XAS spectra were recorded in TFY mode, which uses channeltron to acquire the emitted X-ray photons. All the XAS spectra were measured with a step size of 0.1 eV around the absorption edge jump region that is in accordance with the energy resolution of upstream. The incident photon energy was calibrated by the appropriate reference samples respectively. N K-edge XAS was calibrated with h-BN powder (calibrating the π* peak to 403.5 eV[28, 29]); Al K-edge XAS was calibrated with Al_2O_3 coated Al foil (calibrating the first peak to 1568 eV).

Appendix A. Supplementary material

Supplementary data associated with this article can befound, in the online version.

Notes

The authors declare no competing financial interests.

Acknowledgements

‡ Kaiqi Nie, Hui Zhang and John A. McLeod contributed equally to this work. This work was supported by the Natural Science Foundation of China (NSFC) (Grant No.91333112 and U1432249), the National Key R&D Program of China (Grant 2017YFA0205002), the Priority Academic Program Development of Jiangsu Higher Education Institutions (PAPD). This is also a project supported by Jiangsu Key Laboratory for Carbon-Based Functional Materials and Devices and Collaborative Innovation Centre of Suzhou Nano Science & Technology. The Advanced Light Source is supported by the Director Office of Science, Office of Basic Energy Sciences of the U.S. Department of Energy under Contract No. DE-AC02-05CH11231.

References

[1] J. Lee, T.-H. Han, M.-H. Park, D. Y. Jung, J. Seo, H.-K. Seo, H. Cho, E. Kim, J. Chung, S.-Y. Choi, *Nat. Commun.* **2016**, *7*, 11791. https://doi.org/10.1038/ncomms11791

[2] L. Ke, H. Liu, M. Yang, Z. Jiao, X. Sun, *Chem. Phys. Lett.* **2015**, *623*, 68. https://doi.org/10.1016/j.cplett.2015.01.047

[3] H. Aziz, Z. D. Popovic, N.-X. Hu, A.-M. Hor, G. Xu, *Science* **1999**, *283*, 1900. https://doi.org/10.1126/science.283.5409.1900

[4] J. Lu, A. R. Hlil, Y. Meng, A. S. Hay, Y. Tao, M. D'Iorio, T. Maindron, J.-P. Dodelet, *J. Polym. Sci., Part A: Polym. Chem.* **2000**, *38*, 2887. https://doi.org/10.1002/1099-0518(20000815)38:16<2887::AID-POLA50>3.0.CO;2-F

[5] S. Klod, K. Haubner, E. Jahne, L. Dunsch, *Chem. Sci.* **2010**, *1*, 743. https://doi.org/10.1039/C0SC00350F

[6] M. J. Jurow, A. Bossi, P. I. Djurovich, M. E. Thompson, *Chem. Mater.* **2014**, *26*, 6578. https://doi.org/10.1021/cm503336d

[7] H. Lee, S. W. Cho, Y. Yi, *Curr. Appl. Phys.* **2016**, *16*, 1533. https://doi.org/10.1016/j.cap.2016.09.009

[8] Z. D. Popovic, H. Aziz, N.-X. Hu, A. Ioannidis, P. N. dos Anjos, *J. Appl. Phys.* **2001**, *89*, 4673. https://doi.org/10.1063/1.1354631

[9] K. W. Hershey, J. Suddard-Bangsund, G. Qian, R. J. Holmes, *Appl. Phys. Lett.* **2017**, *111*, 113301. https://doi.org/10.1063/1.4993618

[10] A. Curioni, W. Andreoni, R. Treusch, F. Himpsel, E. Haskal, P. Seidler, C. Heske, S. Kakar, T. Van Buuren, L. J. Terminello, *Appl. Phys. Lett.* **1998**, *72*, 1575. https://doi.org/10.1063/1.121119

[11] P. S. G. Kim, S. J. Naftel, T. K. Sham, I. Coulthard, Y. F. Hu, A. Moewes, J. W. Freeland, *J. Electron. Spectrosc. Relat. Phenom.* **2005**, *144-147*, 901. https://doi.org/10.1063/1.3030975

[12] A. DeMasi, L. F. J. Piper, Y. Zhang, I. Reid, S. Wang, K. E. Smith, J. E. Downes, N. Peltekis, C. McGuinness, A. Matsuura, *J. Chem. Phys.* **2008**, *129*, 224705. https://doi.org/10.1063/1.3030975

[13] K. Takeuchi, S. Yanagisawa, Y. Morikawa, *Sci. Tech. Adv. Mater.* **2006**, *8*, 191. https://doi.org/10.1016/j.stam.2007.01.006

[14] M. Petrosino, A. Rubino, *J. Appl. Phys.* **2012**, *112*, 014504. https://doi.org/10.1063/1.4731719

[15] S. Mizuo, S. Tabatake, S. Naka, H. Okada, H. Onnagawa, *J. Appl. Phys.* **2002**, *92*, 1450. https://doi.org/10.1063/1.1483922

[16] M. Bagge-Hansen, B. C. Wood, T. Ogitsu, T. M. Willey, I. C. Tran, A. Wittstock, M. M. Biener, M. D. Merrill, M. A. Worsley, M. Otani, *Adv. Mater.* **2015**, *27*, 1512. https://doi.org/10.1002/adma.201403680

[17] M. G. Mason, C. W. Tang, L. S. Hung, P. Raychaudhuri, J. Madathil, D. J. Giesen, L. Yan, Q. T. Le, Y. Gao, S. T. Lee, L. S. Liao, L. F. Cheng, W. R. Salaneck, D. A. dos Santos, J. L. Brédas, *J. Appl. Phys.* **2001**, *89*, 2756. https://doi.org/10.1063/1.1324681

[18] F. Li, H. Tang, J. Anderegg, J. Shinar, *Appl. Phys. Lett.* **1997**, *70*, 1233. https://doi.org/10.1063/1.118539

[19] S. Yoshioka, F. Oba, R. Huang, I. Tanaka, T. Mizoguchi, T. Yamamoto, *J. Appl. Phys.* **2008**, *103*, 014309. https://doi.org/10.1063/1.2829785

[20] F. P. Rosselli, W. G. Quirino, C. Legnani, V. L. Calil, K. C. Teixeira, A. A. Leitão, R. B. Capaz, M. Cremona, C. A. Achete, *Org. Electron.* **2009**, *10*, 1417. https://doi.org/10.1016/j.orgel.2009.08.026
[21] P. Ordejón, E. Artacho, J. M. Soler, *Phys. Rev. B* **1996**, *53*, R10441. https://doi.org/10.1103/PhysRevB.53.R10441
[22] J. M. Soler, E. Artacho, J. D. Gale, A. García, J. Junquera, P. Ordejón, D. Sánchez-Portal, *J. Phys.: Condens. Matter* **2002**, *14*, 2745. https://doi.org/10.1088/0953-8984/14/11/302
[23] P. He, F. C. Au, Y. Wang, L. Cheng, C. Lee, S. Lee, *Appl. Phys. Lett.* **2000**, *76*, 1422. https://doi.org/10.1063/1.126051
[24] A. Turak, D. Grozea, X. Feng, Z. Lu, H. Aziz, A.-m. M. Hor, *Appl. Phys. Lett.* **2002**, *81*, 766. https://doi.org/10.1063/1.1494470
[25] S. Meloni, A. Palma, A. Kahn, J. Schwartz, R. Car, *J. Appl. Phys.* **2005**, *98*, 023707. https://doi.org/10.1063/1.1953869
[26] M. Hong, M. K. Ravva, P. Winget, J.-L. Brédas, *Chem. Mater.* **2016**, *28*, 5791. https://doi.org/10.1021/acs.chemmater.6b02069
[27] J. E. Knox, M. D. Halls, H. P. Hratchian, H. B. Schlegel, *PCCP* **2006**, *8*, 1371. https://doi.org/10.1039/B514898G
[28] S. C. Ray, C. W. Pao, H. M. Tsai, J. W. Chiou, W. F. Pong, C. W. Chen, M.-H. Tsai, P. Papakonstantinou, L. C. Chen, K. H. Chen, W. G. Graham, *Appl. Phys. Lett.* **2007**, *90,* 192107. https://doi.org/10.1063/1.2737392
[29] L. Liu, T.-K. Sham, W. Han, *PCCP* **2013**, *15*, 6929. https://doi.org/10.1039/C3CP50498K

ToC figure

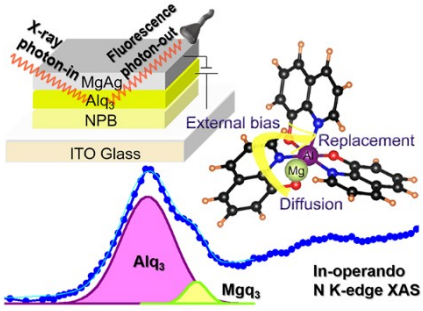
X-ray photon-in
Fluorescence photon-out
MgAg
Alq3
NPB
ITO Glass
External bias
Replacement
Al
Mg
Diffusion
Alq3
Mgq3
In-operando
N K-edge XAS

Supplementary material

Real-time Interface Investigation on Degradation Mechanism of Organic Light-emitting Diode by In-operando X-ray Spectroscopies

Kaiqi Nie, # Hui Zhang, # John A. McLeod, # Duo Zhang, Dongying Zhou, Yujian Xia, Jun Zhong, Liangsheng Liao, Jinghua Guo, and Xuhui Sun**

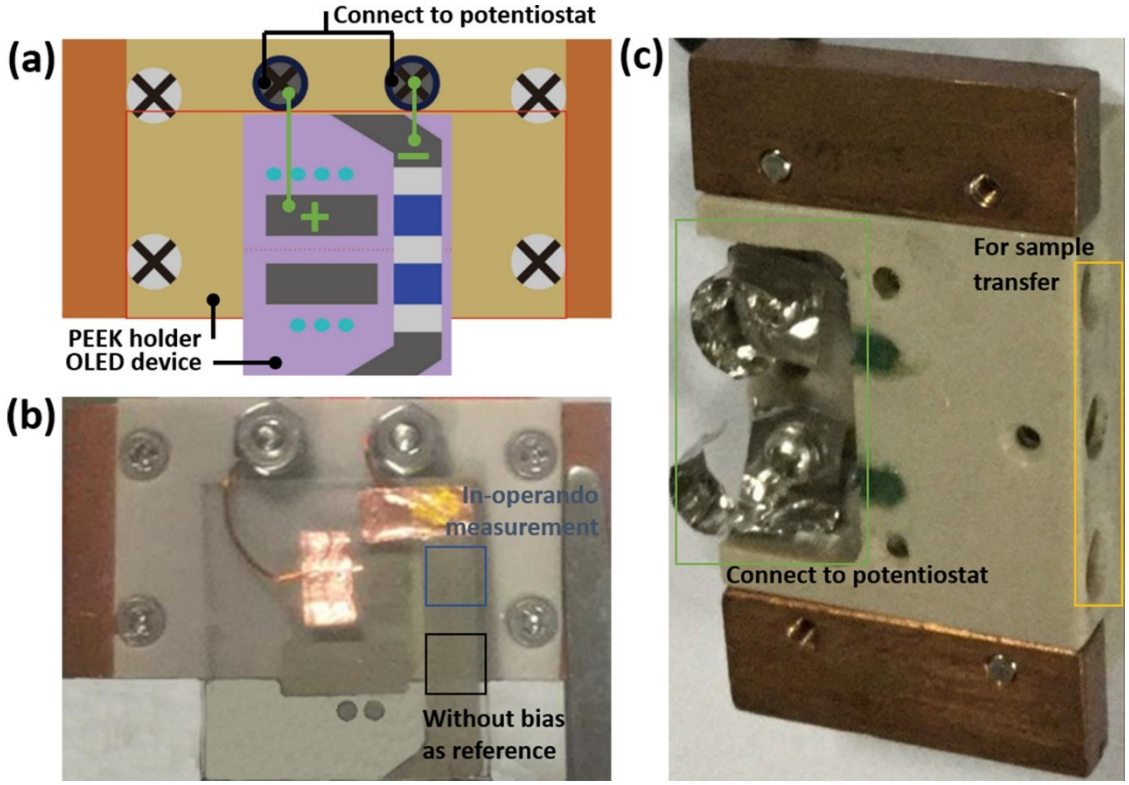

Figure S1. a) Schematic configuration of the sample holder and device assembly for in-operando XAS measurement. b) Photograph of the front side of the in-operando device assembly. c) Photograph of the back side of the in-operando device assembly.

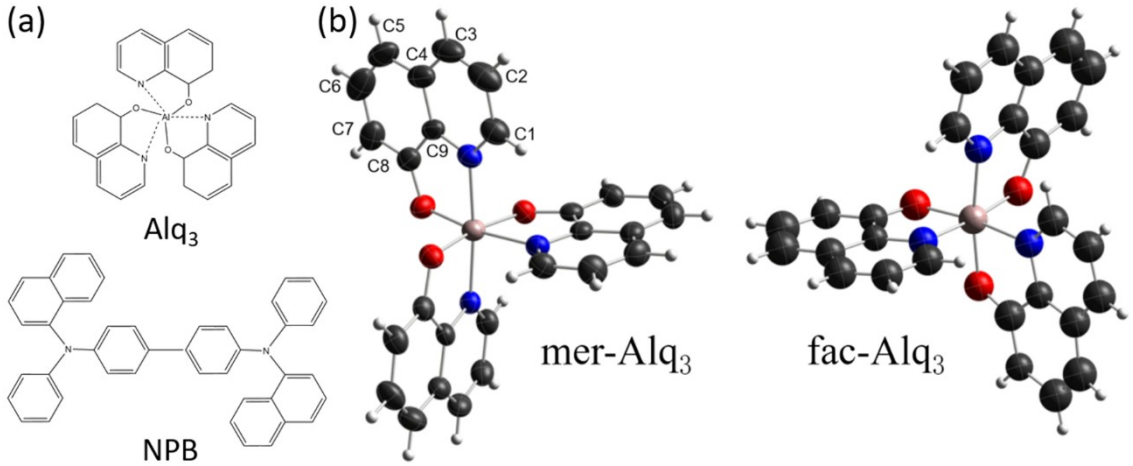

Figure S2. a) Chemical structure of NPB and Alq_3. b) The geometry of mer-Alq_3 and fac-Alq_3 configuration with labels C1-C9 for nine different C atoms in quinoline ligands. Pink, red, blue, black and white balls represent Al, O, N, C and H atoms, respectively.

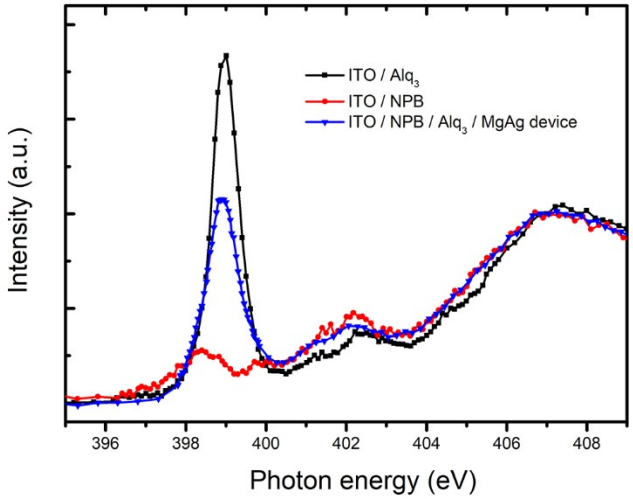

Figure S3. N K-edge spectra comparison of different construction: ITO/Alq_3 (black), ITO/NPB (red), ITO/45 nm NPB/55 nm Alq_3/50 nm MgAg device (blue); All the spectra were normalized at 410 eV.

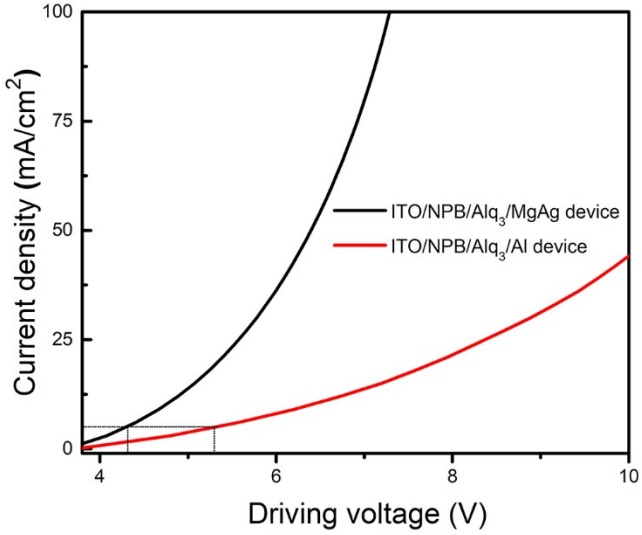

Figure S4. Current-voltage curves of MgAg cathode (black) and Al cathode (red) Alq_3 OLED device.

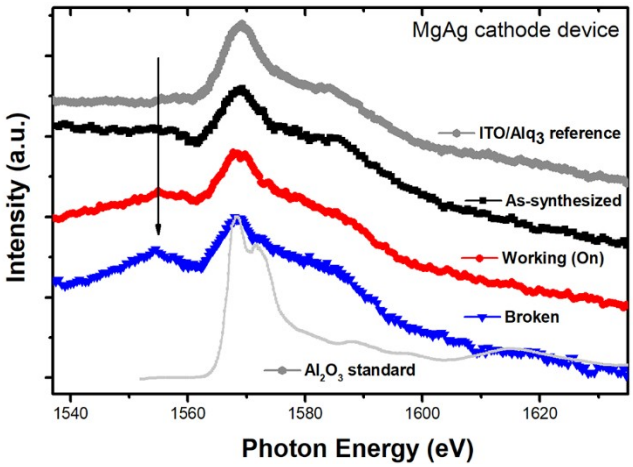

Figure S5. Al K-edge XAS of an Alq_3 film on ITO glass, an as-synthesized ITO/NPB/Alq_3/MgAg OLED device, under bias ("Working (on)"), after failure ("Broken"), and an Al_2O_3 reference standard.

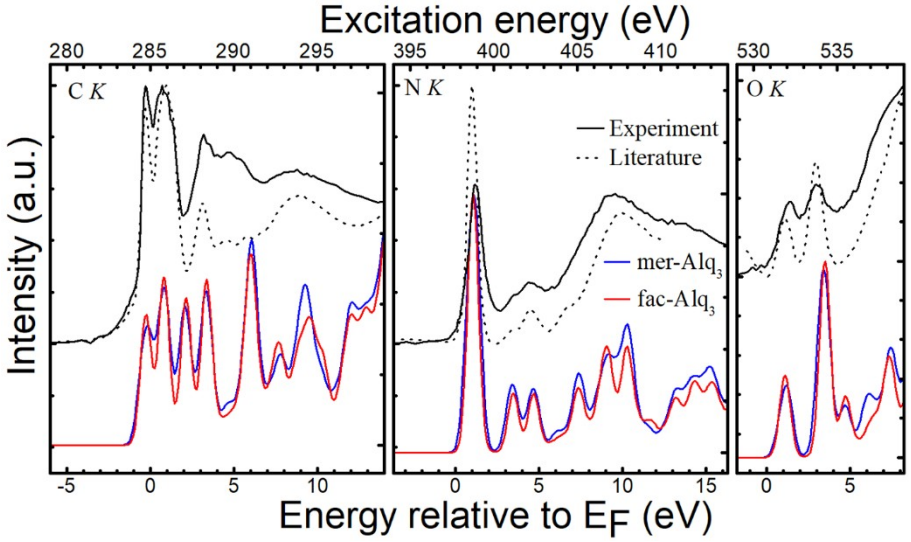

Figure S6. Simulation results of C, N, and O K-edge XAS are shown at the bottom; the experimental and reference spectra from literature is shown in solid and dashed line respectively.

The electronic structures of mer- and fac-Alq_3, mer- and fac-Mgq_3, and a lone Mg near the center of a mer- or fac-Alq_3 molecule were simulated using the SIESTA code.[1, 2] Γ-point calculations were performed with the Lee-Yang-Parr exchange-correlation functional,[3] ultrasoft norm-conserving pseudopotentials, and double-zeta plus polarization basis sets. Atomic coordinates were optimized using the conjugate-gradients method to a force tolerance of 0.04 eV/Å, a plane-wave cutoff of 100 Ry, and a density matrix tolerance of 10^{-4}. The C, N, and O K-edge XANES were simulated using the unoccupied 2p partial density of states.

Charged states were simulated by adding (subtracting) the appropriate integer number of electrons from the system. Because the systems under consideration here are inherently molecular, and we kept the volume per molecule large enough to prevent overlap from adjacent molecules, we avoid the problem of infinite charge which can occur in charged crystalline lattices (due to the inherent periodicity assumed in all DFT calculations). The primary object of these calculations is to simulate the XAS spectrum, and XAS measurements are sufficiently short-ranged such that they only probe the electronic structure of a single molecule, consequently isolating each charged molecule (as opposed to simulating the

crystalline structure of mer- and fac-Alq_3) has a minimal effect on the electronic structures of interest, namely the distribution of unoccupied states ranging up to 15 eV above the Fermi energy.

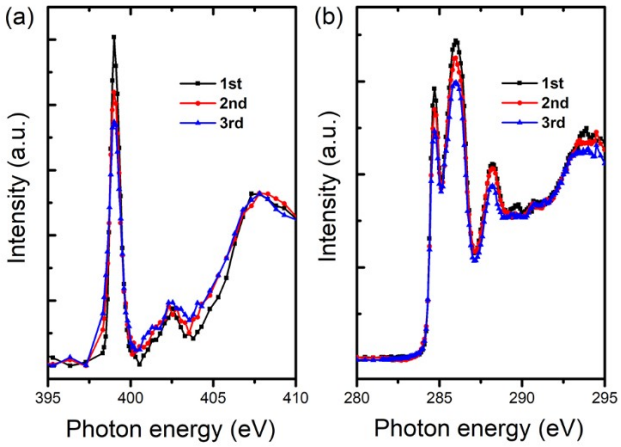

Figure S7. a) N K-edge b) C K-edge XAS of ITO/Alq_3 as a function of X-ray exposure time (1st, 2nd, 3rd scans).

Previous reports have called attention to X-ray induced damage (beam damage) in organic molecules.[4] In order to exclude this possibility from our work, we de-focused the incoming X-ray by tuning the upstream optics to spread the beam spot to 1000×300 µm, which is comparable to the whole device size. Meanwhile, we applied liquid nitrogen cooling to the sample manipulator while acquiring spectra in order to minimize the beam induced thermal damage. We could easily identify that the beam spot is on the light emitting part during the in-operando measurement through the port of the UHV chamber. We did multiple short, successive XAS measurements of the N and C K-edges XAS to ensure that substantial changes in the spectra profiles - indicative of increasing beam damage - did not occur. These spectra profiles are shown in Figure S7. It should be noted that the spectral profile of nitrogen functional groups does evolve slightly with the X-ray exposure time as the absorption intensity decreases gradually at the absorption edge. This phenomenon may be linked to thermal accumulation effect. Importantly, however, these stability tests show that no new features originate from X-ray exposure under our optimized measurement parameter.

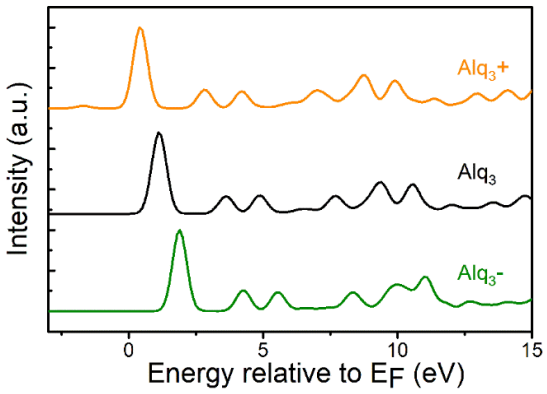

Figure S8. Theoretical N 2p pDOS simulation of an Alq_3 standard (middle); an Alq_3 in positive charge (top); and an Alq_3 in negative charge (bottom). All spectra are shifted vertically for clarity.

X[1] P. Ordejón, E. Artacho, J. M. Soler, *Phys. Rev. B* **1996**, *53*, R10441.

[2] J. M. Soler, E. Artacho, J. D. Gale, A. García, J. Junquera, P. Ordejón, D. Sánchez-Portal, *J. Phys.: Condens. Matter* **2002**, *14*, 2745.

[3] B. Miehlich, A. Savin, H. Stoll, H. Preuss, *Chem. Phys. Lett.* **1989**, *157*, 200.

[4] A. DeMasi, L. F. J. Piper, Y. Zhang, I. Reid, S. Wang, K. E. Smith, J. E. Downes, N. Peltekis, C. McGuinness, A. Matsuura, *J. Chem. Phys.* **2008**, *129*, 224705.